Appl. Phys. A (2017) 123:464
DOI 10.1007/s00339-017-1074-3

Applied Physics A
Materials Science & Processing

CrossMark

Growth of γ-alumina thin films by pulsed laser deposition and plasma diagnostic

K. Yahiaoui[1,3] · S. Abdelli-Messaci[1] · S. Messaoud Aberkane[1] · M. Siad[2] · A. Kellou[3]

Received: 4 January 2017 / Accepted: 31 May 2017 / Published online: 5 June 2017
© Springer-Verlag Berlin Heidelberg 2017

Abstract The present work discusses about the synthesis of alumina thin films, which have applications in current and next-generation solid-state electronic devices due to their attractive properties. Alumina thin films were synthesized by pulsed laser deposition at different oxygen pressures and substrate temperatures. The dependence of substrate temperature, oxygen pressure, and the deposition time on the properties of the films has been observed by growing three series of alumina thin films on Si (100). The first films are synthesized using substrate temperatures ranging from room temperature to 780 °C at 0.01 mbar of O_2. The second series was realized at a fixed substrate temperature of 760 °C and varied oxygen pressure (from 0.005 to 0.05 mbar). The third set of series was elaborated at different deposition times (from 15 to 60 min) while the oxygen pressure and the substrate temperature were fixed at 0.01 mbar and 760 °C, respectively. The films were characterized using X-ray diffractometer (XRD) for structural analysis, a scanning electron microscope for morphological analysis, a nano-indenter for mechanical analysis (hardness and Young's modulus), and Rutherford backscattering spectroscopy for thickness and stoichiometry measurements. Using optical emission spectroscopy, plasma diagnostic was carried out both in the vacuum and in the presence of oxygen with a pressure ranging from 0.01 to 0.05 mbar. Several neutral, ionic, and molecular species were identified such as Al, Al^{+}, and Al^{++} in vacuum and in oxygen ambiance, O and AlO molecular bands in oxygen-ambient atmosphere. The spatiotemporal evolution of the most relevant species was achieved and their velocities were estimated. The highest amount of crystallized alumina in γ-phase was found in the films elaborated under 0.01 mbar of O_2, at a substrate temperature of 780 °C, and a deposition time of 60 min.

✉ K. Yahiaoui
kyahiaoui@cdta.dz

[1] Division Milieux Ionisés & Laser, Centre de Développement des Technologies Avancées, Alger, Algeria

[2] Centre de Recherche Nucléaire d'Alger, 02 Boulevard Frantz Fanon, BP 399 Alger, Algeria

[3] Laboratoire Electronqiue Quantique, Université des Sciences et de la Technologies Houari Boumédiene, Bab-Ezzouar, Algeria

1 Introduction

Pulsed laser deposition (PLD) is one of the promising techniques for the deposition of thin films with complex stoichiometry. It is a flexible, simple, fast, and controllable method for making high-quality thin films, even though the processes involved during laser ablation and film growth are not completely understood. Different materials can be synthesized by PLD such as metallic oxides, high T_c superconductors, ferroelectrics metals, metal compounds, polymers, and biological materials [1, 2]. Alumina is one of these kinds of materials, which has drawn attention due to its interesting properties. It is hard, stable, insulating, and transparent, which allow it to be used for applications in many areas. It owes those properties due to its polymorphism. It can exist in a number of crystalline phases (polymorphs) for instance the gamma series γ, η, θ (metastable structures), and the alpha series κ (metastable) and α (stable). Among these phases, the γ alumina is one of the most important active alumina. It can be found in low temperature and have other technological applications due to its thermal stability [3].

Compared to other alumina film synthesis techniques, such as chemical vapor deposition [4], pulsed direct

magnetron sputtering [5], plasma spraying [6, 7], PLD exhibits several advantages such as the possibility to deposit multi-component films and using low gas pressure. This latter controls the kinetic energy of the particles, which determines the structural and morphological properties of the films. PLD allows also to control the number of particles arriving at the substrate with a specific laser frequency and fluence. Using PLD, alumina thin films have been synthesized under different conditions, using different targets: Al [8, 9], Al_2O_3 target [10–32], Al_2O_3-doped Erbium [26] or Al_2O_3-doped Europium [27], in different ambiances: oxygen [8–24, 26–31], in vacuum [25] or argon [32], and at different substrate's temperatures [24–31] or have been annealed [10, 11, 31]. The films were synthesized in oxygen ambiance at high substrate temperature [24–31] or were annealed after a deposition at room temperature [10, 11]. The most cited works in the literature refer to alumina films in α-, γ- or β-phases [10–12, 25–30] or amorphous [8, 9, 13–21, 31, 32].

For thin film deposition process, plasma study is vital to identify the ablated species, their origin (from laser–target interaction or plasma–gas), and to evaluate their kinetic energy. Several works investigated optical emission spectroscopy diagnostic for aluminum and alumina plasma [8, 23–43]. The effect of laser wavelength has been examined by some authors [34, 38], while others studied the effect of laser fluence at 355 nm [39]. Some works dealt with the effect of oxygen gas [37]. The origin of AlO molecule formation in aluminum and alumina plume induced by laser has been achieved by some authors [35, 41, 42], since this molecule is a precursor to alumina thin film formation.

In our previous work [43], the alumina thin film deposition has not been achieved after the dynamic of alumina plasma study. This is due to alumina target's small size which induces deep drilling of the target and the no conservation of the ablation condition, when using high substrate temperature and long deposition time, required for Al_2O_3 thin film synthesis.

In the present work, a new target with large size and high purity of 99.99% has been used for this task. An optimization of the experimental conditions, such as gas pressure, substrate temperature, and deposition time is investigated for alumina thin films. Two applications of the synthesized alumina thin films were targeted; to be used as a buffer layer for its catalytic property (γ phase) and protective layer for its mechanical properties. The substrate temperature and the kinetic energy of the species are the key parameters to synthesize thin films with the cited properties (γ phase and mechanical properties) but the substrate heating system in the laboratory has a limitation of 800 °C. For this reason, a relatively high laser fluence is used as a supplementary substrate heating source, where the energetic species will impinge the substrate and increase the surface substrate mobility. The elaborated films from polycrystalline α-Al_2O_3 target ablated by a KrF laser at 10 J/cm^2 were characterized by X-ray diffractometer (XRD) for structural analysis. We used a scanning electron microscope (SEM) for morphological analysis, nano-indenter for mechanical analysis, and RBS for thickness measurements and stoichiometry. Moreover, alumina plasma emission spectroscopy has been conducted in different oxygen pressures and the molecular AlO formation has been discussed. A correlation between the nature of the films and the species velocities was also investigated.

2 Experimental setup

PLD experiments were performed using a KrF excimer (Lambda Physik COMPex 102) laser ($\lambda = 248$ nm and $\tau = 25$ ns) which was focused on a rotating polycrystalline ceramic α-alumina target ($\phi = 60$ mm, 99.99% purity acquired from Goodfellow and more pure than that used in our previous paper (89.54%) [43]). We report in Fig. 1 the structural and optical properties of the target.

The schematic experimental setup can be found elsewhere [47]. For the structural and crystallinity of the films, XRD (Bruker D8 Advance) has been used in grazing incidence geometries. The surface morphology of the films was examined with a SEM (Jeol JSM-6360 LV). The mechanical measurements were carried out with nano-indenter (CSM instruments) which is equipped with a Berkovich diamond indenter tip. The RBS experiments were performed using a beam of 2 MeV He+ particles, delivered by the Van de Graff 3.75 MV accelerator of the CRNA (Centre de Recherche Nucléaire d'Alger). The backscattered particles were detected at 160° scattering angle.

3 Results and discussion

3.1 The choice of laser fluence

The major problem encountered in thin film synthesis by PLD is the presence of droplets at higher laser fluence. These droplets are formed due to phase explosion phenomenon [2, 44–47], recoil pressure [2], hydrodynamical instabilities, and exfoliation [48]. For this reason, a detailed study has been carried out by varying ablated mass versus laser fluence. The choice of relatively high laser fluence is limited by the laser fluence threshold where the phase explosion mechanism occurs.

Notice that the variation of the ablated mass versus laser fluence for the first alumina target [43] is different from that

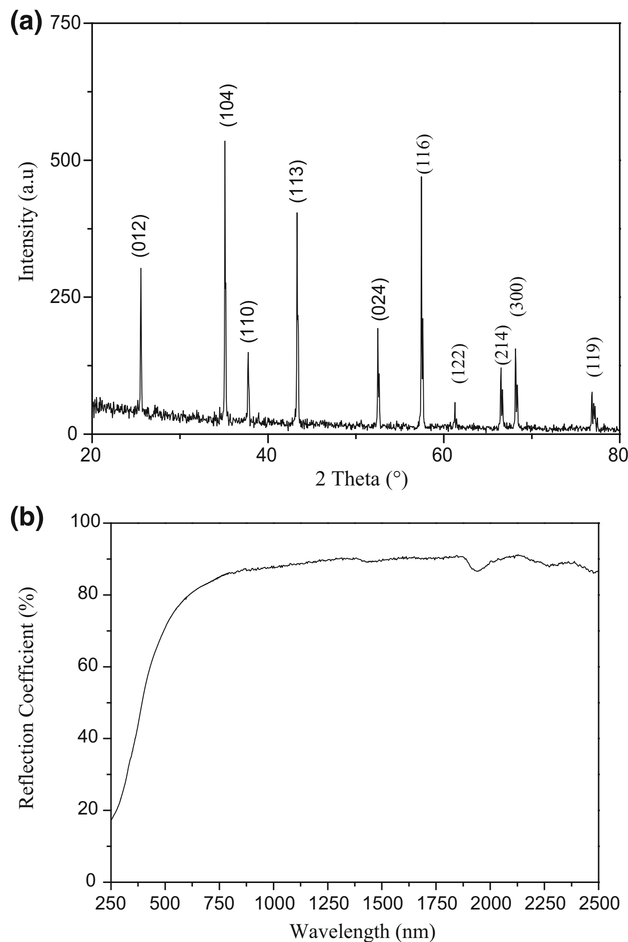

Fig. 1 Characterization of the alumina target. **a** XRD analysis, **b** spectrophotometer analysis

of the present target [47]. Depending upon laser fluence range the mechanisms of ablation are different. The choice of the laser fluence at 10 J/cm^2 permits an important ablation rate and energetic species below the phase explosion. The energetic species can enhance the surface mobility as well as the sticking and nucleation rate at the substrate surface [49] to compensate the limited heating system in temperature.

3.2 Film deposition

At 4 cm from the target, several thin films of Al_2O_3 were deposited on Si (100) for different oxygen pressures (0.05–0.005 mbar), different substrate temperatures (from room temperature to 780 °C), and different deposition time (15–60 min).

3.2.1 XRD analysis

The effect of the substrate temperature on the microstructural properties of alumina films at 0.01 mbar of O_2 with a deposition time of 15 min is also investigated. Generally, the appropriate pressure for oxide thin films deposition by PLD is around this value. Figure 2 shows the XRD patterns of Al_2O_3 thin films carried out at a substrate temperature ranging from 600 to 780 °C. The films were amorphous for a substrate temperature below 600 °C. Their crystallization began from a substrate temperature higher than 650 °C. The identified peaks at 45.87° and 66.89° (2θ) correspond to reflections from (400) and (440) planes, respectively. Those peaks match well with the cubic structure of γ-phase of alumina. As the substrate temperature increases, the integrated intensity of the peak at 66.89° (440) also increases, indicating more crystallized films.

To show the effect of O_2 pressure on the crystallinity of alumina films, we have fixed the substrate temperature at 760 °C and deposition time to 15 min and varied O_2 pressure from 0.005 to 0.05 mbar. The films were amorphous for 0.05 mbar and crystallized below this value. The highest integrated intensity of the peak at (440) was obtained for 0.01 mbar (see Fig. 3).

Pillonnet et al. have obtained crystallized alumina films at 0.001 mbar of O_2, at a substrate temperature of 790 °C, and a fluence of 3 J/cm^2 using a KrF laser [24]. For the same laser fluence, Cibert et al. have synthesized Al_2O_3 films in γ phase at 800 °C in vacuum [25]. Balakrishnan et al. found crystallized Al_2O_3 at 700 °C and 0.003 mbar of O_2 pressure [26, 28–30]. The crystallinity of their films deposited on Si (100) matches with the γ-phase structure. All the authors observed peaks corresponding to the reflection of (400) and (440). In addition, Pillonnet et al. [24] and Cibert et al. [25] observed a supplementary peak due to the reflection of (311). Furthermore, the reflection of (511) was observed by Cibert et al.

Pillonnet et al. and Cibert et al. using the same mode of heating (halogen lamp) also found that the substrate temperature to get a detectable crystallite is 790 °C [24] and

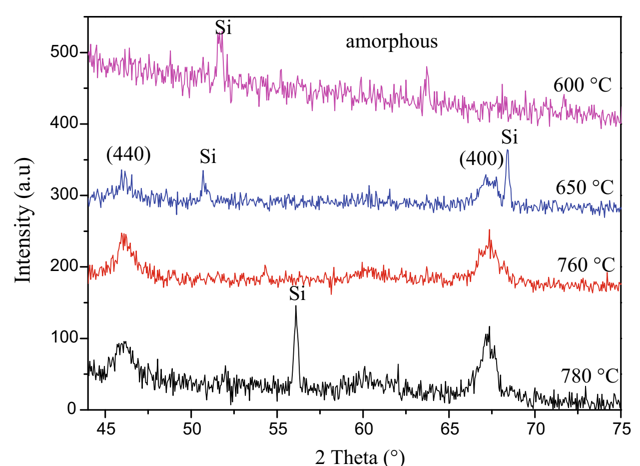

Fig. 2 XRD patterns of Al_2O_3 thin films deposited on Si (100) at 0.01 mbar and different substrate temperatures

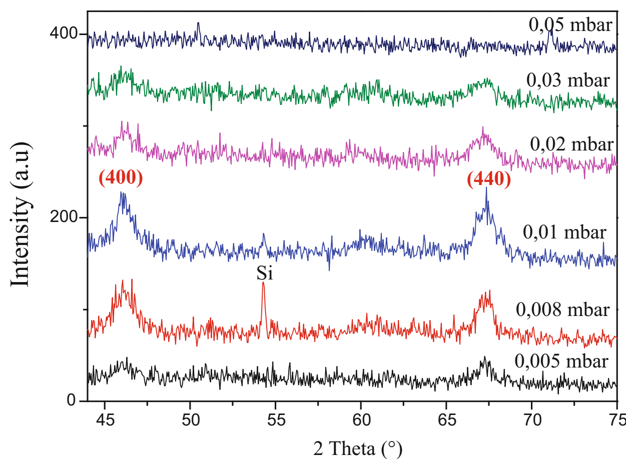

Fig. 3 XRD spectrum of Al_2O_3 thin films deposited on Si (100) at substrate temperature of 760 °C and different O_2 pressures

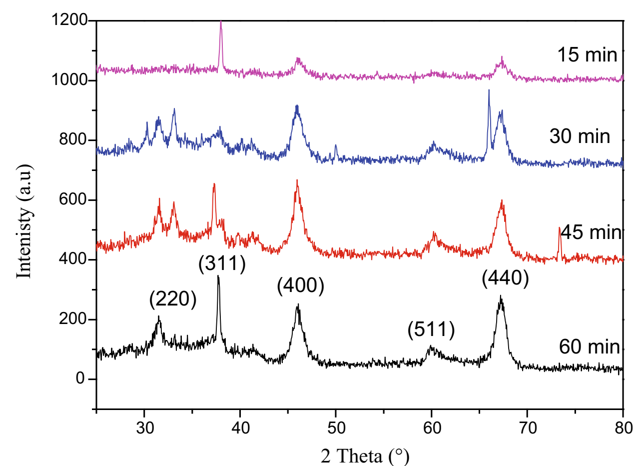

Fig. 4 XRD patterns of Al_2O_3 thin films deposited on Si (100) at $P(O_2) = 0.01$ mbar, substrate temperature of 760 °C, and different deposition times

800 °C [25], respectively, whereas Balakrishnan et al. observed crystallinity at 700 °C [26, 28–30]. The authors reported [24, 26, 28–30] that the intensities of their peaks increased with decreasing gas pressure.

In the present work, for a fluence of 10 J/cm^2, the beginning of crystallization onto the γ-phase is observed for a substrate temperature of 650 °C for peaks at 45.87° and 66.89° (2θ), with a deposition time of 15 min less than that used by Pillonnet et al. (45 min) and Balakrishnan et al. (60 min). As reported by the authors [24, 26, 28–30], the films became more crystallized when the processing gas pressure decreases. Moreover, the optimum pressure of O_2 was found at 0.003 mbar [26, 28–30] and 0.001 mbar [24] for 3 J/cm^2. In this study, the crystallized films were obtained at 0.01 mbar. In fact, the kinetic energy of the ablated species increases with laser fluence, while a decrease is observed with the gas pressure increase. It, also, enhances the surface mobility, the sticking, and nucleation rate at the substrate surface [48]. This explains the increase in the optimum of O_2 pressure in the present work.

To study the effect of deposition time on the structure of Al_2O_3, several films were deposited on Si (100) varying from 15 to 60 min. The substrate temperature and O_2 pressure were fixed at 760 °C and 0.01 mbar, respectively. Figure 4 shows the XRD patterns of the films at different deposition times. The intensities of the peaks related to the reflection of (400) and (440) plans increase with increasing the deposition time. Other peaks from the reflections of (311) and (511) planes started to be visible at 30 min and also their intensities was found to increase with deposition time. By increasing the deposition time, the amount of crystallized matter increases too.

3.2.2 SEM analysis

The SEM analysis has been performed to show the morphology of alumina films under several substrate temperatures and 0.01 mbar of O_2 (Fig. 5). At 500 and 600 °C, where the films are amorphous, their surfaces seem to be granular with the presence of dispersed droplets. In addition, as the substrate temperature increases, the films are crystallized and their surfaces exhibit the presence of island growths. Their numbers increased with the rise in substrate temperature possessing sizes between 100 nm and 1 μm. The reason could be the increase in temperature (growth mechanism) rather than laser–target interaction. The growth mode could be the Stranski–Krastanov mode [50] which is defined as a mixed growth from layer and islands. The latter have a conical shape, different from the droplets (spherical).

However, the observed droplets in amorphous films were assigned to splashing, exfoliation or hydrodynamical instabilities as reported in our previous contribution [47] and the articles therein; they are due to laser–target interaction.

As reported in previous work [47] droplets and islands favor the thermoluminescent (TL) response of the films [19] which can be used as UV or beta-detectors [18].

At a laser fluence of 3 J/cm^2, Balakrishnan et al. [30] observed a smooth and structureless morphology of alumina films deposited on Si (100) with some droplets assigned to exfoliation and surface boiling.

3.2.3 RBS analysis

RBS analysis has been conducted for the crystalline films prepared at 760 °C and an oxygen pressure ranging from

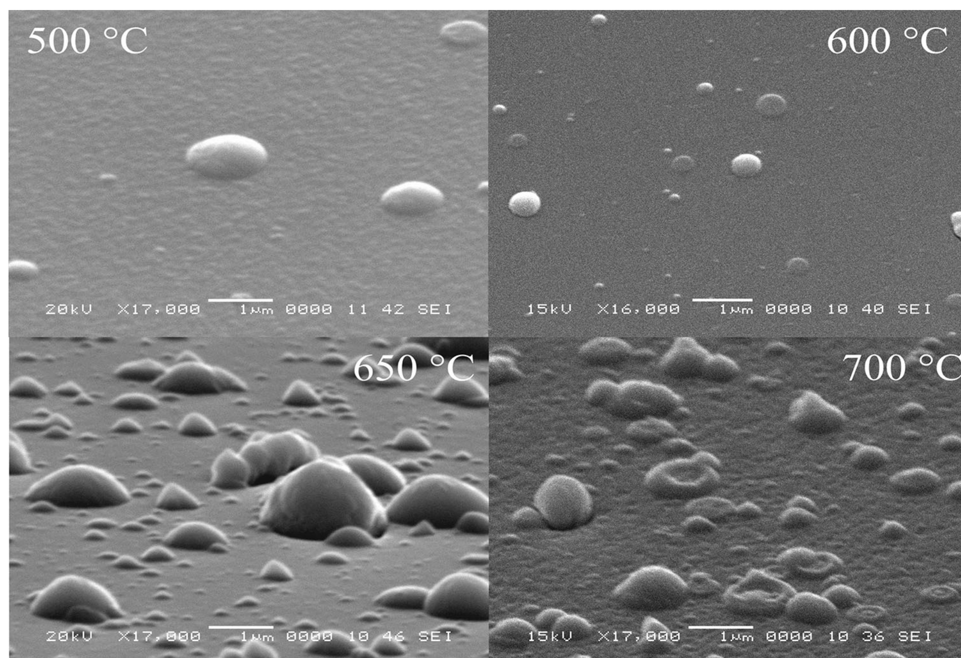

Fig. 5 SEM images of Al_2O_3 thin films for $P(O_2) = 0.01$ mbar and different substrate temperatures

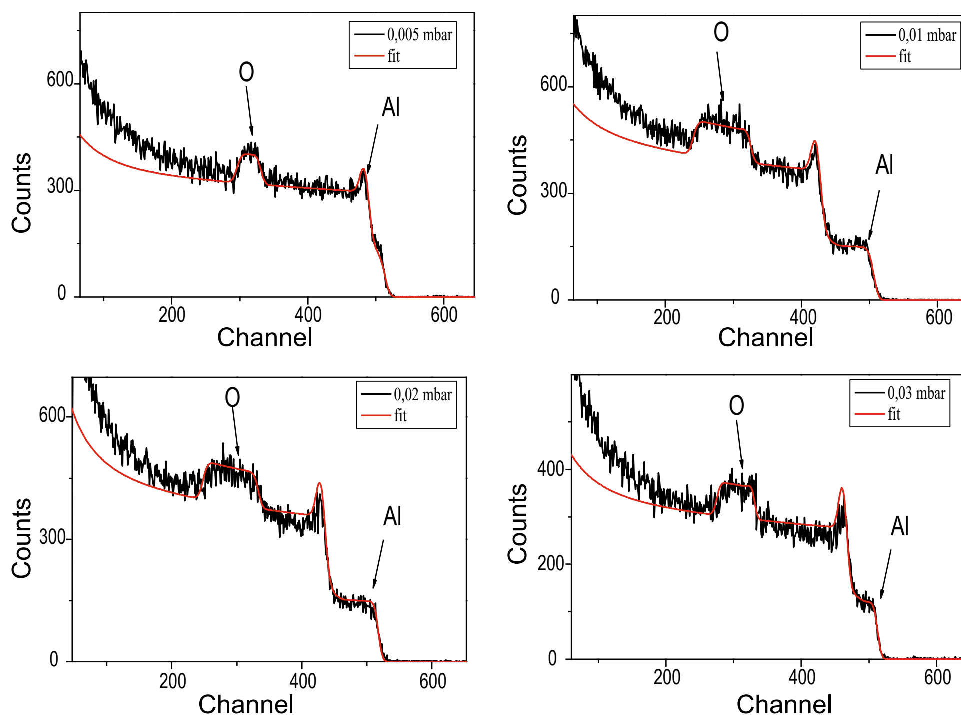

Fig. 6 RBS spectra for different O_2 pressures

0.005 to 0.03 mbar. In Fig. 6, we report the typical RBS spectra which have been used to fit the composition and the thickness of the films assuming a density of 3.6 g/cm^3 for γ phase [24]. The simulation of the spectra was achieved using the SIMNRA program [51]. The chemical ratio O/Al for each pressure is presented in Fig. 7. All the film compositions are oxygen richness with a particularity for the films at 0.02 mbar which have a composition close to the stoichiometry of alumina (1.5). Pillonnet et al. and Cibert et al. found a stoichiometry of 1.5 (Al_2O_3) for their films at 790 °C with specific oxygen pressure [24] and in vacuum at RT [25]. A slight excess in oxygen is also observed for 800 °C [25].

The thickness variation as function of oxygen pressure can be observed from Fig. 8. Taking into account the estimated error bars, the maximum thickness is obtained

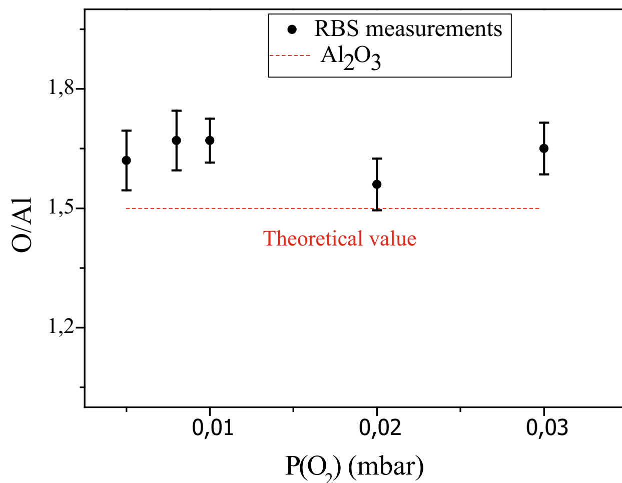

Fig. 7 Stoichiometry of alumina thin films as function of O_2 pressure

for 0.01 and 0.02 mbar, where the plasma confinement and geometry are at their optimum. The results suggest that the film thicknesses are governed not only by the fluence of the ablating laser pulse, but also by the interaction between the plasma constituents and the reactive gas. The O_2 pressure strongly affects the laser plasma plume dynamics such as expansion velocity, species distributions in the plume, and dissociation process which influence the films properties.

Notice that the error bar of the thickness is estimated from the statistical error of the counting and the error bar on the ratio (O/Al) is estimated from the sum of the statistical errors calculated from the areas (counts) of the peaks of O and Al, in the RBS spectrum.

3.2.4 Nanoindentation study

Nanoindentation measurements were carried out to find the nano-hardness and elastic modulus of Al_2O_3 films deposited at 0.01 mbar of O_2 and at different substrate temperatures as reported in Fig. 9.

The results showed that the increase of the substrate temperature induces an increase in the nano-hardness and the Young modulus of the films (Fig. 9). Nath et al. [31] corroborate these results where the nano-hardness and the Young modulus increase with temperature and reached a maximum of 21 and 28 GPa, respectively, at an annealing temperature of 1000 °C. Others [29] found a nano-hardness of about 20.8 and 24.7 GPa for RT and 700 °C, respectively. In this work, the nano-hardness varies from 13.6 to 27.7 GPa and the Young's modulus varies from 119.73 to 173.22 GPa between 500 and 780 °C. With such a nano-hardness order of magnitude, alumina films have potential application in hard and wear-resistant coatings.

Moreover, from XRD patterns we have calculated the crystallite size using the Scherrer equation from the (400) reflection for different thin films:

$$D = \frac{K\lambda}{\Delta(2\theta)\cos(\theta)}, \tag{1}$$

where D is the crystallite size, K is a dimensionless shape factor of 0.9, λ is the instrument wavelength of 0.15406 nm, $\Delta(2\theta)$ is the line broadening at half the maximum intensity (FWHM) in radians, and θ is the Bragg diffraction angle.

The crystallite size was 10.53, 8.54, and 7.44 nm for 650, 688, and 780 °C, respectively. Balakrishnan et al. [29] found a crystallite size of 10 nm for 700 °C and 0.035 mbar of O_2. We noticed that the substrate temperature is inversely proportional to the crystallite size. Thereby, the nano-hardness is also inversely proportional to crystallite size. In bulk material, it is well known that the decrease of crystallite size increases the presence of joints in the material causing an increase of micro-hardness [52, 53].

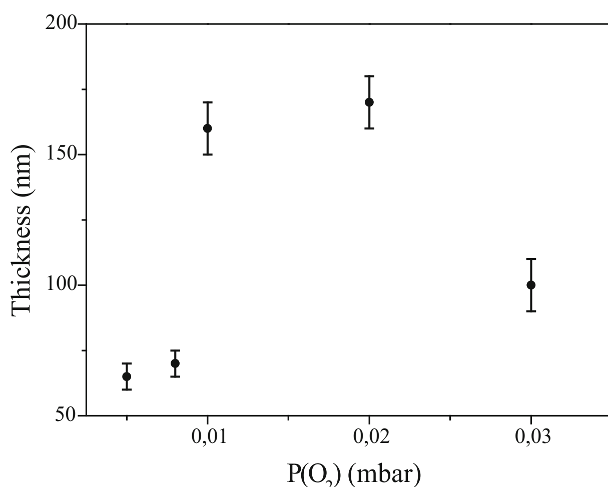

Fig. 8 Thickness of alumina thin films as function of O_2 pressure

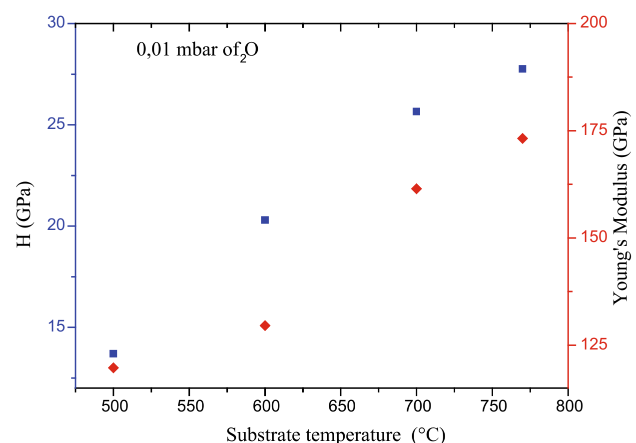

Fig. 9 Nano-hardness and elastic Young modulus of Al_2O_3 films at 0.01 mbar of O_2 versus substrate temperature

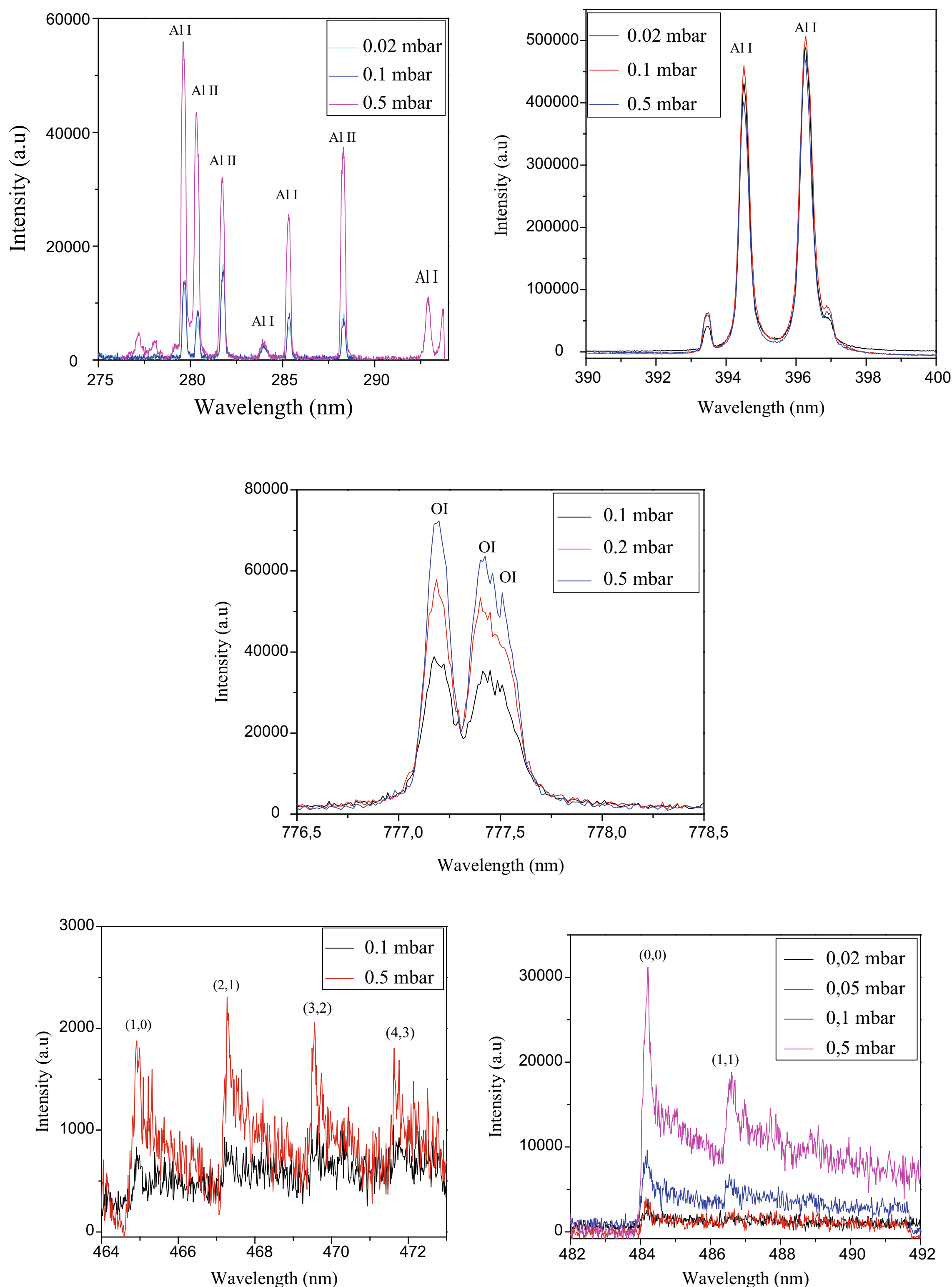

Fig. 10 Alumina plasma emission spectra at 3 mm from the target surface and for different O_2 pressures

3.3 Optical emission spectroscopy analysis

To understand the physico-chemical process involved in the interaction between alumina plasma and oxygen gas (excitation, dissociation, and recombination), optical emission spectroscopy has been conducted. More precisely, OES spectroscopy has been performed to identify the excited species in the plume, which are precursors for

alumina film growth. The origin of the species can be deduced from their spatiotemporal evolution (from the target surface or formed in gas phase) and an estimation of their kinetic energy can inform us on the kinetic energy range that favors the formation γ-Al_2O_3 phase.

To identify the excited species constituting the plasma, integrated plasma emission spectra were recorded between 200 and 780 nm, at 3 mm from the target surface in vacuum and under different oxygen gas pressure from 0.01 to 5 mbar.

The most important lines presented in the plasma plume have been identified using the NIST database [54]. The spectra show several atomic and ionic emission lines Al I, Al II, and Al III in vacuum. The strongest emission from Al I lines occurred at 396.15 nm and 309.27 nm, while the most intense emissions from Al II were observed at 281.61, 466.30, and 358.65 nm. A weak emission of Al III species appeared at a wavelength of 318.01 nm.

In oxygen ambiance, in addition to aluminum lines emissions, emission of the AlO molecular band was recorded for the sequence $\Delta v = 0$ and $\Delta v = 1$ with a threshold pressure of 0.02 and 0.05 mbar, respectively. The emission of the triplet lines of neutral oxygen was also observed at 777.19, 777.41, and 777.53 nm. As the oxygen pressure increases, the intensity of all the species in the plume increases, indicating more excitation and thus more interaction of the plasma species with the surrounding gas molecules as shown in Fig. 10.

Optical times of flight (TOF) profiles of Al III, Al II, Al I, O I, and the (0,0) band head of AlO at respective wavelengths 318.01, 281.65, 396.15, 777.19, and 484.21 nm were investigated in vacuum and in O_2 gas pressure of 0.01, 0.02, and 0.05 mbar, to obtain their spatiotemporal evolution as reported in Fig. 11. In Table 1, we report the species velocities in the different ambiance, which decrease with O_2 pressure increasing. At 0.01 mbar of O_2 no oxygen excited species were recorded in the spectrum. For 0.02 and 0.05 mbar, neutral oxygen appears and follows the spatiotemporal evolution of Al I species. The fastest species evolved in the plasma were the ions of aluminum, viz., Al^{++} and the Al^{+} followed by Al and O. The slowest species was molecular band head AlO.

The evolution of the Al line intensities as function of distance for different O_2 pressures is illustrated in Fig. 12.

Table 1 Linear velocities of plasma species in vacuum and under 0.01, 0.02 and 0.05 mbar in the early stages of expansion

Species	V (10^6 cm/s)					
	Al I	Al II	Al III	O I		AlO
Pressure (mbar)						
2×10^{-5}	1.66	2.57	4.41			
0.01	1.58	2.47	4.02			1.054
0.02	1.46	2.43	3.91	1.54	1.91	0.817
0.05	1.27	2.25	3.54	1.47	1.87	0.799

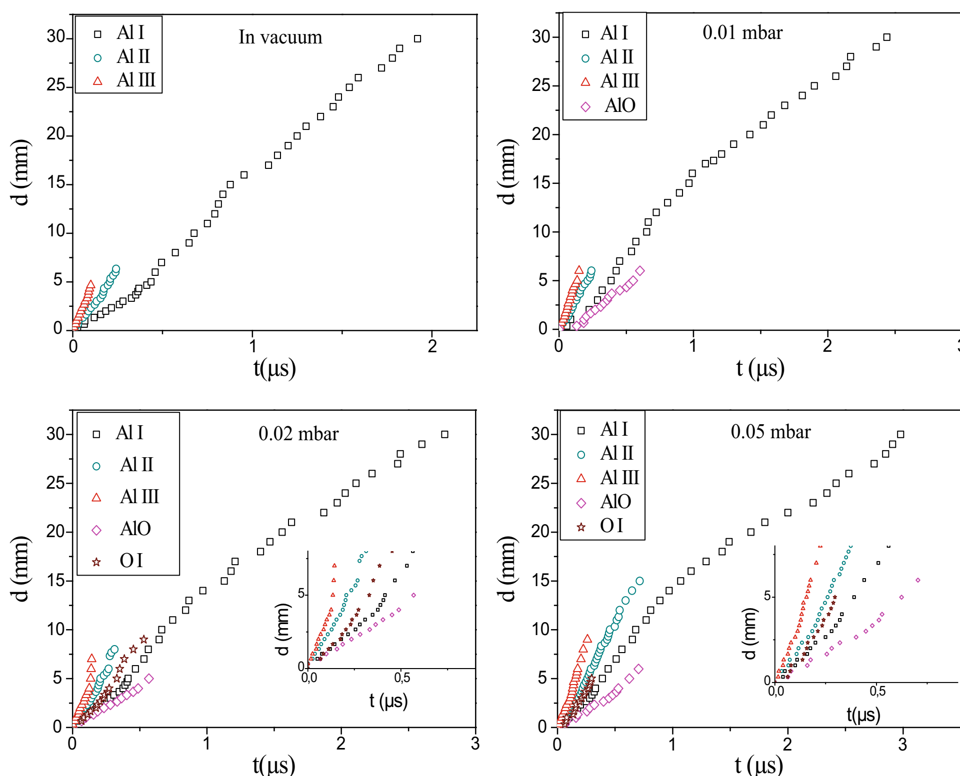

Fig. 11 Spatial–temporal evolution of Al III, Al II, Al I, O I, and AlO in vacuum and under 0.01, 0.02, and 0.05 mbar of O_2

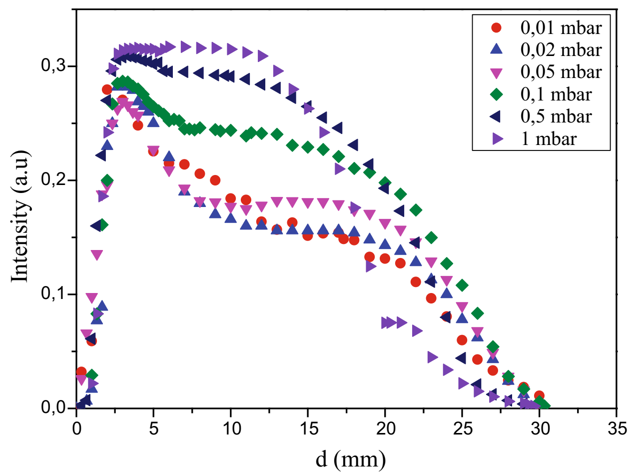

Fig. 12 The evolution of Al I intensity as function of distance from the target for different O_2 pressures

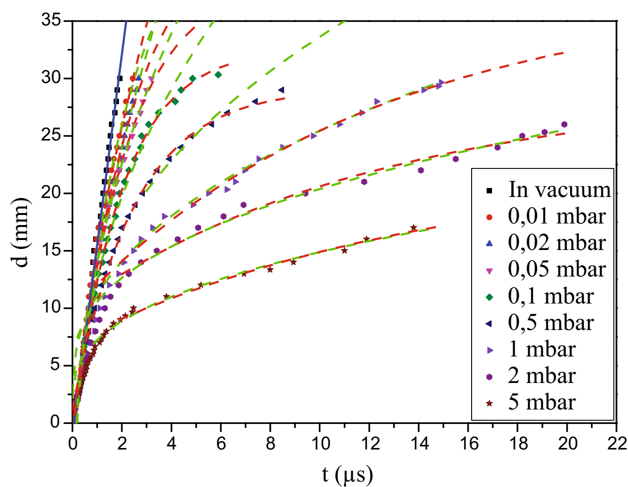

Fig. 13 Spatiotemporal evolution of Al I (396.15 nm) in vacuum and for different oxygen gas pressures: *red* and *green dashed lines* represent the fit with drag and shock wave models, respectively, and the *blue line* represents the linear fit

For each pressure, the line intensity of Al species increased during their expansion in the plasma, showing re-excitation under collisions. Besides, as the oxygen pressure increased, the Al intensity increased showing a more excited species due to pressure confinement.

From the spatiotemporal evolution, we notice that the AlO is originated from the laser–target interaction, since they are the slowest species. In vacuum, the AlO molecule is probably present, may be too weak to be detected. However, Salik et al. [38] recorded the emission of AlO band head in vacuum using a visible and infrared laser. In fact, the plasma is more heated and the species are more excited due to the Bremsstrahlung inverse process which is more efficient in plasma induced with infrared than UV laser. This can explain why AlO is not observed in our study in vacuum and low O_2 pressure.

To study the dynamics of plasma, we have chosen the most intense species of plasma for oxygen pressure ranging from 0.01 to 5 mbar. The spatiotemporal evolution of Al I (396.15 nm) is reported in Fig. 13. Two models are used: the first is the drag model, where the position of the plasma R can be estimated using the following relation $R = R_0(1 - e^{-\beta t})$, where R_0 is the stopping distance and β is the slowing coefficient [33, 55]. The second is the shock wave model. It follows the form $\xi_0(E_0/\rho_0)\ t^{2/5}$, where ξ_0 depends on the specific heat capacity denoted γ. The shock model describes the explosive release of energy E_0 from the plasma plume through a background gas density ρ_0 [55]. These models have been used when an injected surrounding gas interacts with the plume. The Al(I) species expand freely in vacuum. But in the presence of oxygen at early stages of expansion, the species expands freely as in vacuum followed by a shockwave expansion model. At later stages, the species expansion is described by the drag model. The fit with drag and shock wave model is represented in Fig. 13.

From the drag model, the stopping distance of the Al(I) species is determined. This is useful when choosing the substrate–target distance. But this latter is always taken from the stopping distance of the plasma front (for more details refer the article [43]) than from the neutral Al which is not the farthest species in the plume. Notice that even if the excited ionized Al^{++} and Al^{+} do not reach a far distance in their expansion when compared to the excited neutral Al I (Fig. 11) but when using a Langmuir probe in a previous work [47], the ions have achieved a distance of 14 cm of these species in vacuum. Furthermore, the drag model is more suitable to describe the expansion of the plasma for intermediate and high gas pressure (above 0.1 mbar). In this case, the estimated stopping distances are more reliable than those for lower pressure (below 0.01 mbar). The drag model does not fit well the expansion for the lower pressure (below 0.1 mbar), for this reason the estimated stopping distances are not accurate.

We report in Table 2 the stopping distances and the ejected velocities for Al I (396.15 nm) derived from the drag model fit for 5, 2, 1, 0.1, 0.5, 0.05, 0.02, and 0.01 mbar.

The most relevant result is: as the pressure increases the species velocities decrease. Two parameters are responsible for this increase: the laser fluence and the gas pressure.

For the adopted laser fluence (10 J/cm^2), the crystallized films were obtained with a pressure 0.01 mbar of O_2, while in the other literature it is found with different parameters such as using laser fluence about times lesser than ours, i.e., 3 J/cm^2, 0.001 mbar pressure and temperature 700 °C [24–26]. Our laser fluence is three times higher. We are

Table 2 Stopping distances and the ejected velocities for Al I (396.15 nm) at different oxygen pressures

Gas pressure (mbar)	Stopping distance (mm)	Ejected velocities ($10^6 \times$ cm/s)
0.01	47.84	1.87
0.02	45	1.84
0.05	39.48	1.80
0.1	33.45	1.66
0.5	28	1.27
1	27.8	0.23
2	18.78	0.15
5	15.68	0.10

expecting that the crystallization would begin at substrate temperature lower than 650 °C when increasing deposition time (more than 15 mn). The results show a shift in the substrate temperature and gas pressure due to the choice of a relatively high laser fluence of 10 J/cm^2. The increase in laser fluence increases ablation rate and the kinetic energy of ions and atoms arriving at the substrate surface. The sticking and nucleation rate as well as the surface mobility then increase, favoring the crystallization at lower substrate temperature and deposition time. The substrate temperature, the oxygen pressure, and the laser fluence are important parameters that determine alumina films' crystallinity.

4 Conclusion

In contrast to the past literature experimental conditions [24, 25], crystallized films are formed using higher laser fluence 10 J/cm^2 and less heating of the substrate. The film morphology and nano-hardness are found to be different and it mainly depends on the fluence parameter. The optimum for crystallized films in γ-phase was found to be at a higher oxygen pressure and a lower substrate temperature compared to films at lower laser fluence.

The XRD analysis data show that the peak intensities and their integrals are significant for an optimum O_2 pressure of 0.01 mbar and the substrate temperature of 780 °C.

Alumina thin film morphology shows a difference between amorphous and crystallized films. For this latter, the appearance of islands growing from the film surface is observed much clearly.

The RBS analysis shows that all the films possess oxygen richness except the films at 0.02 mbar which have a stoichiometry close to the Al_2O_3. The nanoindentation tests indicate that as the substrate temperature increases, the nano-hardness and Young's modulus also increase, reaching a value of 27.7 and 173 GPa, respectively, for 780 °C. The optical emission spectroscopy diagnostic of the plume at different oxygen pressures allowed us to have a range of kinetic energy values that favors the films' crystallization for the chosen laser fluence.

Acknowledgements The authors are thankful for the help with the language of the manuscript rendered by Ashwin kumar Myakalwar, Post Doc at Institute of Photonics and Electronics, Czech Academy of Sciences, Prague and by researchers from CDTA and USTHB, Algeria: Ratiba Fellag, Nadjet Bouhelal, and Rachda-Habiba Benhagouga.

References

1. D.B. Chrisey, G.K. Hubler, *Pulsed Laser Deposition of Thin Films* (Wiley, New York, 1994)
2. D. Bauerle, *Laser Processing and Chemitry*, 4th edn. (Springer, Berlin, 2011)
3. Y. Wang, J. Wang, M. Shen, W. Wang, J. Alloy. Compd. **467**, 405 (2009)
4. T. Maruyama, T. Nakai, Appl. Phys. Lett. **58**(19), 2079 (1991)
5. S.K. Pradhan, P.J. Reucroft, Y. Ko, Surf. Coat. Technol. **176**, 382 (2004)
6. R. Krishnan, S. Dash, R. Kesavamoorthy, C. Babu Rao, A.K. Tyagi, B. Raj, Surf. Coat. Technol. **200**, 2791 (2006)
7. R. Krishnan, S. Dash, R.K. Sole, A.K. Tyagi, B. Raj, Surf. Eng. **18**(3), 208 (2002)
8. A. Misra, R.K. Thareja, Appl. Surf. Sci. **143**, 56 (1999)
9. A. Misra, H.D. Bist, M.S. Navati, R.K. Thareja, J. Narayan, Mater. Sci. Eng. B **79**, 49 (2001)
10. B. Hirschauer, S. Söderholm, J. Paul, A.S. Flodström, Appl. Surf. Sci. **99**, 285 (1996)
11. B. Hirschauer, S. Söderholm, G. Chiaia, U.O. Karlsson, Thin Solid Films **305**, 243 (1997)
12. P.-H. Haumesser, J. Théry, P.-Y. Daniel, A. Laurent, J. Perrière, R. Gomez-San Roman, R. Perez-Casero, J. Mater. Chem. **7**(9), 1763 (1997)
13. J. Gottmann, A. Husmann, T. Klotzbücher, E.W. Kreutz, Surf. Coat. Technol. **100–101**, 415 (1998)
14. A. Husmann, J. Gottmann, T. Klotzbücher, E.W. Kreutz, Surf. Coat. Technol. **100–101**, 411 (1998)
15. E.W. Kreutz, J. Gottmann, Phys. Status Solidi (a) **166**, 569 (1998)
16. J. Gottmann, E.W. Kreutz, Surf. Coat. Technol. **116–119**, 1189 (1999)
17. J. Gottmann, G. Schlaghecken, E.W. Kreutz, Appl. Phys. A **69**, S597 (1999)
18. J.E. Villarreal-Barajas, L. Escobar-Alarcón, E. Camps, P.R. González, E. Villagrán, M. Barboza-Flores, Superficies y Vacio **13**, 126 (2001)

19. L. Escobar-Alarcón, E. Villagrán, E. Camps, S. Romero, J.E. Villarreal-Barajas, P.R. González, Thin Solid Films **433**(1–2), 126 (2003)
20. A. Suárez-García, J. Gonzalo, C.N. Afonso, Appl. Phys. A **77**(6), 779 (2003)
21. P. Katiyar, C. Jin, R.J. Narayan, Acta Mater. **53**, 2617 (2005)
22. R. Serna, M. Jiménez de Castro, J.A. Chaos, A. Suárez-Garcia, C.N. Afonso, M. Fernández, I. Vickridge, J. Appl. Phys. **90**(10), 5120 (2001)
23. G. Wang, O. Marty, C. Garapon, A. Pillonnet, W. Zhang, Appl. Phys. A **79**, 1599 (2004)
24. A. Pillonnet, C. Garapon, C. Champeaux, C. Bovier, R. Brenier, H. Jaffrezic, J. Mugnier, Appl. Phys. A **69**, S735 (1999)
25. C. Cibert, H. Hidalgo, C. Champeaux, P. Tristant, C. Tixier, J. Desmaison, A. Catherinot, Thin Solid Films **516**, 1290 (2008)
26. G. Balakrishnan, P. Kuppusami, S. Tripura Sundari, R. Thirumurugesan, V. Ganesan, E. Mohandas, D. Satikumar, Thin Solid Films **518**, 3898 (2010)
27. M. Ion, C. Berbecaru, S. Iftimie, M. Filipescu, M. Dinescu, S. Antohe, Dig. J. Nanomater. Biostruct. **7**(4), 1609 (2012)
28. G. Balakrishnan, S. Tripura Sundari, R. Ramaseshan, R. Thirumurugesan, E. Mohandas, D. Satikumar, P. Kuppusami, T.G. Kim, J.I. Song, Ceram. Int. **39**(8), 9017 (2013)
29. G. Balakrishnan, R. Venkatesh Babu, K.S. Shin, J.I. Song, Opt. Laser Technol. **56**, 317 (2014)
30. G. Balakrishnan, R. Thirumurugesan, E. Mohandas, D. Satikumar, P. Kuppusami, J.I. Song, J. Nanosci. Nanotechnol. **14**, 7728 (2014)
31. S. Nath, I. Manna, S.K. Ray, J.D. Majumdar, Ceram. Int. **42**(6), 7060 (2016)
32. R. Boidin, T. Halenkovič, V. Nazabal, L. Beneš, P. Němec, Ceram. Int. **42**(1), 1177 (2016)
33. S.S. Harilal, C.V. Bindhu, M.S. Tillack, F. Najmabadi, A.C. Gaeris, J. Appl. Phys. **93**(5), 2380 (2003)
34. N.M. Shaikh, S. Hafeez, B. Rashid, M.A. Baig, Eur. Phys. J. D **44**, 371 (2007)
35. C.H. Ching, R.M. Gilgenbach, J.S. Lash, J. Appl. Phys. **78**(5), 3408 (1995)
36. H. Furusawa, T. Sakka, Y.H. Ogata, Appl. Phys. A **79**, 1291 (2004)
37. L. Escobar-Alarcón, A. Arrieta, E. Camps, S. Romero, M. Fernandez, E. Haro-Poniatowski, Appl. Phys. A **93**, 605 (2008)
38. M. Salik, M. Hanif, M.A. Baig, IEEE Trans. Plasma Sci. **39**(9), 1861 (2011)
39. C. Ursu, O.G. Pompilian, S. Gurlui, P. Nica, M. Agop, M. Dudeck, C. Focsa, Appl. Phys. A **101**, 153 (2010)
40. A.D. Handoko, P.S. Lee, P. Lee, S.R. Mohanty, R.S. Rawat, J. Phys. **28**, 100 (2006)
41. S.S. Harilal, B.E. Brumfield, B.D. Cannon, M.C. Phillips, Anal. Chem. **88**(4), 2296 (2016)
42. J. Hermann, A. Lorusso, A. Perrone, F. Strafella, C. Dutouquet, B. Torralba, Phys. Rev. E **92**, 053103 (2015)
43. K. Yahiaoui, S. Abdelli-Messaci, S. Messaoud-Aberkane, T. Kerdja, H. Kellou, Spectrochim. Acta B **93**, 20 (2014)
44. K. Yahiaoui, T. Kerdja, S. Malek, Surf. Interface Anal. **42**, 1299 (2010)
45. J.H. Yoo, O.V. Borisov, X. Mao, R.E. Russo, Anal. Chem. **73**(10), 2288 (2001)
46. M. Stafe, I. Vladoiu, I.M. Popescu, Cent. Eur. J. Phys. **6**(2), 327 (2008)
47. K. Yahiaoui, S. Abdelli-Messaci, S. Messaoud Aberkane, A. Kellou, Appl. Phys. A **122**, 963 (2016)
48. A. Bogaerts, Z. Chen, R. Gijbels, A. Vertes, Spectrochim. Acta B **58**, 1867 (2003)
49. J. Schou, Appl. Surf. Sci. **255**, 5191 (2009)
50. G.H. Gilmer, M.H. Grabow, JOM **39**(6), 19 (1987)
51. M. Mayer, AIP Conf. Proc. **475**, 541 (1999)
52. S. Messaoud Aberkane, A. Bendib, K. Yahiaoui, S. Boudjemai, S. Abdelli-Messaci, T. Kerdja, S.E. Amara, M.A. Harith, Appl. Surf. Sci. **301**, 225 (2014)
53. A. Leyland, A. Matthews, Wear **246**, 1 (2000)
54. http://physics.nist.gov/cgi-bin/ASD/lines1.pl
55. D.B. Geohegan, Thin Solid Films **220**, 138 (1992)